

Nonequilibrium Spectral Evolution of Sub-Kondo Resonance

Jong E. Han*

Department of Physics, State University of New York at Buffalo, Buffalo, New York 14260, USA

(Dated: March 19, 2025)

Numerical renormalization group (NRG) is formulated for nonequilibrium steady-state by converting finite-lattice many-body eigenstates into scattering states. Extension of the full-density-matrix NRG for a biased Anderson impurity model reveals the sub-Kondo spectral evolution in the zero-temperature limit, exposing the double-resonance structure at bias of the Kondo energy scale T_K . The sub-Kondo peaks result in population inversion due to the lead-resolved resonance and the negative differential conductance regime at temperatures $T \ll T_K$, which revert to the conventional thermal behavior at $T \lesssim T_K$.

Formulation of nonequilibrium statistical mechanics for biased quantum systems has been a tremendous challenge in recent decades. In nonequilibrium quantum many-body theories, much of the focus has been placed on quantum impurity models [1–11] as the prototype strong correlation model and its pivotal role for solving the condensed matter limit through the dynamical mean-field theory [12, 13]. Despite the huge effort, the theoretical rigor and the numerical efficiency of the nonequilibrium impurity solvers have yet to reach a satisfactory level at which the techniques are routinely applicable to nonequilibrium lattice calculations.

The Kondo problem [1, 2] remains as the testbed of various strongly correlated nonequilibrium that led to analytical theories [3, 4], diagrammatic methods [5, 6, 14], real-time simulation [7], imaginary-time simulation [8, 15], numerical renormalization group (NRG) [11], and auxiliary density-matrix method [9, 10]. The debate on how the Kondo resonance dissipates under bias, namely whether the main Kondo peak splits into a double-peak with its spacing equal to the bias, has largely been confirmed. However, computational difficulties have limited the understanding of what happens to the Kondo singlet when it breaks into a double-peak with its energy scale in the sub-Kondo regime. It is the purpose of this work to provide clarity by building on the well-established NRG method with minimal extensions for steady-state nonequilibrium.

The model of an Anderson impurity coupled to the source (or left, L) and drain (or right, R) reservoirs can be written with the Hamiltonian

$$\hat{H} = \sum_{\sigma} \epsilon_f n_{f\sigma} + U \left(n_{f\uparrow} - \frac{1}{2} \right) \left(n_{f\downarrow} - \frac{1}{2} \right) \quad (1)$$

$$+ \sum_{\alpha k \sigma} \epsilon_k c_{\alpha k \sigma}^{\dagger} c_{\alpha k \sigma} - \frac{t}{\sqrt{\Omega}} \sum_{\alpha k \sigma} (f_{\sigma}^{\dagger} c_{\alpha k \sigma} + c_{\alpha k \sigma}^{\dagger} f_{\sigma}),$$

with the creation/annihilation operators $f_{\sigma}^{\dagger}/f_{\sigma}$ for the impurity f -orbital of spin $\sigma = \uparrow, \downarrow$, and $c_{\alpha k \sigma}^{\dagger}/c_{\alpha k \sigma}$ for the conduction electrons with the continuum index k and the reservoir index $\alpha = L, R$. The impurity occupation number (per spin) is $n_{f\sigma} = f_{\sigma}^{\dagger} f_{\sigma}$, U the Coulomb repulsion parameter and ϵ_f the impurity level-energy. The contin-

uum energy for the reservoirs ϵ_k is assumed to be independent of α and σ for simplicity. We further assume that ϵ_k forms a flat density of states with the bandwidth D . We set $D = 1$ as the unit of energy. The mixing of f -orbital with the conduction band, given as t (with the normalization factor Ω), is parametrized by the hybridization parameter $\Gamma_{\alpha} = \pi t^2 \Omega^{-1} \sum_k \delta(\epsilon_k)$. In this work, we focus on the symmetric coupling $\Gamma_L = \Gamma_R$ and define the total hybridization as $\Gamma = \Gamma_L + \Gamma_R$. We use the convention $\hbar = e = k_B = 1$ with the Planck constant \hbar , electric charge e , and the Boltzmann constant k_B .

The steady-state nonequilibrium density-matrix $\hat{\rho}_{\text{neq}}$ driven by the chemical potential difference, $\mu_L = V/2$ and $\mu_R = -V/2$, is constructed as

$$\hat{\rho}_{\text{neq}} = \frac{1}{Z} e^{-\beta(\hat{H} - V\hat{Y})} \quad \text{with } \beta = 1/T, \quad (2)$$

where Hershfield's Y -operator [16]

$$\hat{Y} = \frac{1}{2} \sum_{k\sigma} (\psi_{Lk\sigma}^{\dagger} \psi_{Lk\sigma} - \psi_{Rk\sigma}^{\dagger} \psi_{Rk\sigma}) \quad (3)$$

is constructed from the full scattering-state operators $\psi_{\alpha k \sigma}^{\dagger}$ to the Hamiltonian \hat{H} through the Lippmann-Schwinger equation [8, 15, 17, 18] that contains the interacting system and the reservoirs. $Z = \text{Tr} e^{-\beta(\hat{H} - V\hat{Y})}$ is the normalization constant so that $\text{Tr} \hat{\rho}_{\text{neq}} = 1$. With $\psi_{\alpha k \sigma}^{\dagger}$ being energy eigen-operators of \hat{H} , the density-matrix $\hat{\rho}_{\text{neq}}$ is time-independent with the multiple chemical potentials defined from electron reservoirs. Despite its deceptively simple form, application of the formulation has been much limited since its construction requires the knowledge of the full eigen-operators. The numerical renormalization group (NRG) theory [11, 19–21] iteratively constructs the low-energy many-body eigenstates and presents a promising possibility that may build scattering-states to an interacting Hamiltonian and a steady-state density-matrix.

Before implementing the NRG for the nonequilibrium steady-state, we first discuss how finite-lattice eigenstates can be used to represent scattering states. As illustrated in Fig. 1(a), eigenstates for a system made up of two leads (depicted as lines) and a quantum dot (black dot)

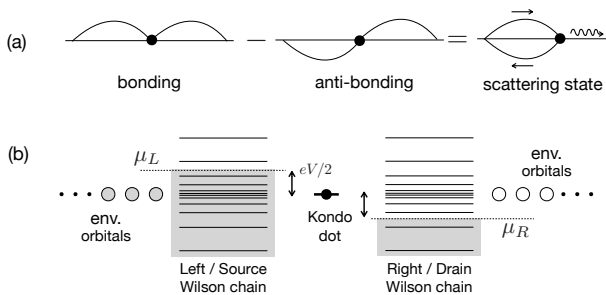


FIG. 1. The nonequilibrium NRG scheme for an Anderson impurity coupled to biased reservoirs. The L/R reservoir is made up of the Wilson chain of length N with the $N_{\max} - N$ environment orbitals at energy levels at zero. The chemical potentials apply up to $\pm V/2$ to L/R -reservoirs, respectively, including the environment orbitals. The levels from the Wilson chains follow the conventional scaling of the Wilson tight-binding parameters.

can be understood as a bonding or an anti-bonding state with nearly degenerate energies in the tunneling regime. By forming a certain linear combination between them, we can create a right- or left-moving scattering state, as depicted. While this is not an exact eigenstate, we take that as an approximate eigenstate of an open system. The explicit construction follows the general scattering theory [18],

$$\hat{Y} = \frac{i\eta}{-\mathcal{L} + i\eta} \hat{Y}_0, \quad (4)$$

where the initial Y -operator \hat{Y}_0 is that of disconnected leads and impurity [i.e., $t = 0$ in Eq. (1)], therefore trivially constructed under any bias as $\hat{Y}_0 = \frac{1}{2}(\hat{N}_L - \hat{N}_R)$ with $\hat{N}_\alpha = \sum_{k\sigma} c_{\alpha k\sigma}^\dagger c_{\alpha k\sigma}$. The Liouvillian \mathcal{L} acting on the operator space is defined as $\mathcal{L}\hat{A} = [\hat{H}, \hat{A}]$ for an arbitrary operator \hat{A} . With energy eigenstates $|\alpha\rangle$ and $|\beta\rangle$ of the total \hat{H} , the full Y -operator can be written as

$$\langle\alpha|\hat{Y}|\beta\rangle = \frac{i\eta}{-E_\alpha + E_\beta + i\eta} \langle\alpha|\hat{Y}_0|\beta\rangle. \quad (5)$$

It is immediately clear that \hat{Y} is Hermitian with $\mathcal{L}^\dagger = -\mathcal{L}$. The infinitesimal factor η sets the time scale η^{-1} over which a scattering state is established [18].

The infinitesimal factor η , set as finite during numerical calculations, plays two crucial roles: (1) η anneals any operator into an eigen-operator of the full Hamiltonian within the energy shell within η , (2) Within the shell, it mixes eigenstates of a finite-lattice into approximate scattering states as depicted in Fig. 1(a). Therefore, η should be chosen as small but finite enough to mix the bonding and anti-bonding states.

To test the concept Eq. (4) for a DC transport, we perform an elementary calculation of the non-interacting

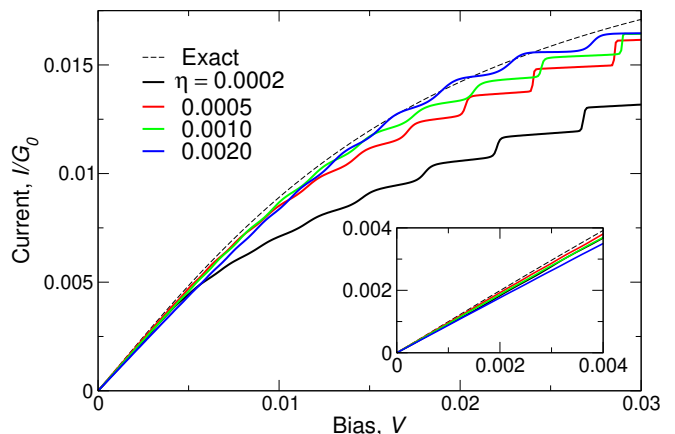


FIG. 2. Current calculated in the non-interacting resonant level model. The current expectation value I (per spin, see text for definition) scaled with the conductance quantum $G_0 = e^2/(2\pi\hbar)$ follows the exact result (dashed line) in the low bias limit (blown up in the inset). The infinitesimal factor η is varied for $\eta \ll t$ with $t = 0.05$. The level energy is set to the particle-hole symmetric limit $\epsilon_f = 0$.

resonant-level (NIRL) model [Eq. (1) with $U = 0$] where the states $|\alpha, \beta\rangle$ in Eq. (5) can be represented by single-particle basis. We model the reservoirs by the Wilson chain (WC) [19–21] to densely sample the low-lying states as depicted in Fig. 1(b). The L/R reservoirs are modeled with respective WC having the number of sites $N_W = 80$, and the renormalization factor $\Lambda = 1.2$. The WCs can be easily diagonalized in the single-particle basis, and through Eqs. (2) and (5), it is straightforward to set up the nonequilibrium density-matrix and we may evaluate the current expectation value by using any single-particle theory. The code that produced Fig. 2 is provided in Supplementary Material (SM) [22].

The comparison of this method shown against the exact result [23] (dashed line in Fig. 2) demonstrates the validity of Hershfield’s density-matrix [16] through Eq. (4) with the current $\langle I \rangle = it/(2\sqrt{\Omega}) \sum_k \text{Tr} \hat{\rho}_{\text{neq}} (c_{Rk\sigma}^\dagger f_\sigma - c_{Lk\sigma}^\dagger f_\sigma + H.C.)$. Following the steps of Eqs. (2-5), one can construct the density-matrix and evaluate any steady-state observables. Regardless of the η values, the linear transport region agrees well with the linear response limit for the current (per spin) $I = G_0 V$ with the unitary quantum conductance $G_0 = 1/(2\pi)$. As the bias increases, the discreteness of the finite WC becomes apparent and the results start to deviate from the exact result $I = (\Gamma/\pi) \tan^{-1}(V/2\Gamma)$ as η becomes too small. This demonstration shows that the nonequilibrium density-matrix can be formulated with the Y -operator, Eq. (4).

In the interacting limit $U > 0$, we use the full-density-matrix NRG (FDM-NRG) [24, 25] to incorporate the nonequilibrium excitations. As depicted in Fig. 1(b), the reservoir is made up of the WC and the environ-

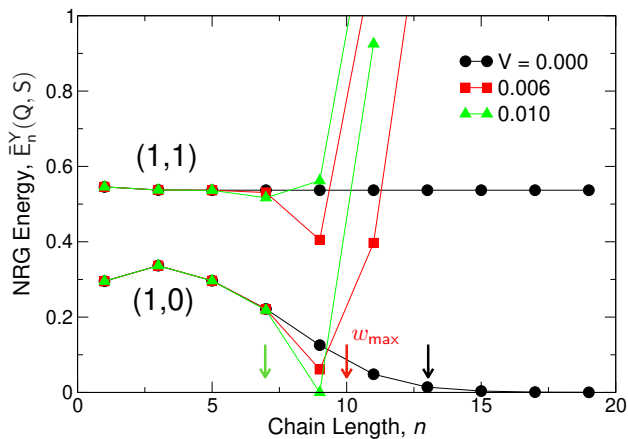


FIG. 3. RG flow of eigenvalues of $(\hat{H} - V\hat{Y})/D_n$ per (Q, S) at (odd integer) chain lengths n , $\bar{E}_n^Y(Q, S)$, with bias up to $V/2 \sim T_K$. Q and S are charge and spin quantum numbers from the equilibrium ground state (with $t = 0$), and D_n is the RG energy scale, Eq. (7). The $(1, 0)$ sector, Kondo-screened doubly-occupied impurity, approaches the Kondo fixed point at $V = 0$. As the bias grows, the RG flow strongly departs from the fixed point at the chain length (indicated by an arrow for each bias with corresponding color) that gives the maximum density-matrix weight.

ment orbitals. The FDM-NRG uses the complete set of the Hilbert space of the WC of maximum length by keeping record of the NRG-truncated states. The formulation of the FDM-NRG remains unchanged except that the steady-state density-matrix Eq. (2) is non-diagonal with the eigenstates of \hat{H} within the energy shell of width η . The algorithm of building the reduced density-matrix [25, 26] remains unchanged from the equilibrium NRG. One simple, yet crucially different step is the proper consideration of the free-energy contribution from the environment orbitals under bias. The environment orbitals, despite being disconnected from the WC, are also subject to the bias and the increase of the WC length (i.e. the decrease of the environmental orbitals) by one site leads to the partition function $Z_{\text{env}} = [(1 + e^{V/2T})(1 + e^{-V/2T})]^2$ and the free-energy change from the environment variables

$$\Delta F_{\text{env}} = V + 4T \ln(1 + e^{-V/2T}). \quad (6)$$

The factor $e^{-\Delta F_{\text{env}}/T}$ is multiplied to the density-matrix Eq. (4) at each NRG iteration. The configurational weight w_n in the FDM thus obtained peaks sharply [25] at the WC length $n = M$ reasonably well predicted by the condition of the NRG energy scale D_n ,

$$D_M \approx V/2 \text{ with } D_n = \Lambda^{-(n-1)/2}, \quad (7)$$

with the NRG renormalization factor Λ (See SM [22]).

Fig. 3 shows the RG flow of the eigenvalues E_n^Y of the (statistical) energy $\hat{H} - V\hat{Y}$ of the WC length n ,

renormalized by the scale D_n . The model parameters are $U = 1$, $\Gamma = 0.1$, and in the particle-hole symmetric limit ($\epsilon_f = 0$). The NRG parameters are as follows throughout this work unless mentioned otherwise: $\Lambda = 4$, the number of kept states $N_{\text{kept}} = 1200$. With two chains, each NRG iteration has the Hilbert space of dimension $16 \times N_{\text{kept}}$ on which \hat{H} and $\hat{\rho}_{\text{neq}}$ are computed. The total charge and spin (Q, S) defined from the equilibrium ground state are conserved quantum numbers. At zero bias $V = 0$, the (spin-singlet) doubly-occupied impurity state, $(1, 0)$, approaches the Kondo fixed-point as $n \rightarrow \infty$ with its energy converging to the ground state energy of $(0, \frac{1}{2})$. As the bias is applied, the flow strongly deviates from the fixed-point starting at $n \approx M$. The M values for the maximum weight w_M are marked by arrows for each bias. The calculation shows that physical observables have the dominant contribution when the system is about to depart from the fixed-point.

We now turn to the crucial discussions of spectral evolution under bias. The procedures for the spectral function calculation are identical to those of the equilibrium FDM-NRG with the density-matrix given by Eqs. (2) and (4). In practice, due to the rapid growth of the Hilbert space with two WCs, the number of kept states N_{kept} is limited and it has to be carefully checked that we sample the bias energy window of $(-V/2, V/2)$ sufficiently. At the iterations of the maximum FDM weight w_{max} , $E_{\text{kept}}/(V/2) \sim 5 - 10$ with the maximum kept energy E_{kept} (See SM [22] for details). The difference between $N_{\text{kept}} = 900$ and 1200 was insignificant. We used the usual log-gaussian spectral summation [21, 27] with the broadening factor of 0.44, after which a uniform gaussian smoothing is performed [25] with the width $\delta = 0.2 \times \max(T_K, T, V/2)$. The Kondo temperature T_K is estimated [2, 28] as $T_K = \sqrt{U\Gamma/2} e^{-1/J}$ with $J = (2/\pi)\Gamma(|\epsilon_f - U/2|^{-1} + |\epsilon_f + U/2|^{-1})$. We performed the z -averaging [29] with $N_z = 8$.

Figs. 4(a)-(c) present spectral functions of the particle-hole (p-h) symmetric Anderson model under bias in the strong Kondo regime $U/\Gamma = 10$ with $T_K/\Gamma = 0.044$. The spectral functions are computed by using the so-called self-energy trick [30] and denoted as $\rho^\Sigma(\omega)$. It is well-known that $\rho^\Sigma(\omega)$ is numerically more reliable than that from the direct spectral summation $\rho(\omega)$. The right-inset in (a) illustrates the sharpness of the Kondo resonance at zero bias compared to the charge peaks at $\omega = \pm U/2$. The main plot in (a) shows the spectral evolution of the Kondo resonance for low bias up to $V = 0.04$, much less than $\Gamma = 0.1$. The spectrum at zero bias (black) has the resonance at $\rho^\Sigma(0) \approx 1/(\pi\Gamma)$, satisfying the unitary limit, and its width well matching the estimated T_K as well. In the low-temperature limit ($T = 0.0005 \ll T_K$), the Kondo resonance is barely affected at low bias $V \ll T_K$. When the (half) bias matches $V/2 \approx T_K$, the Kondo resonance goes through a rapid evolution with a sharp dip at $\omega = 0$. We emphasize that to resolve the low-

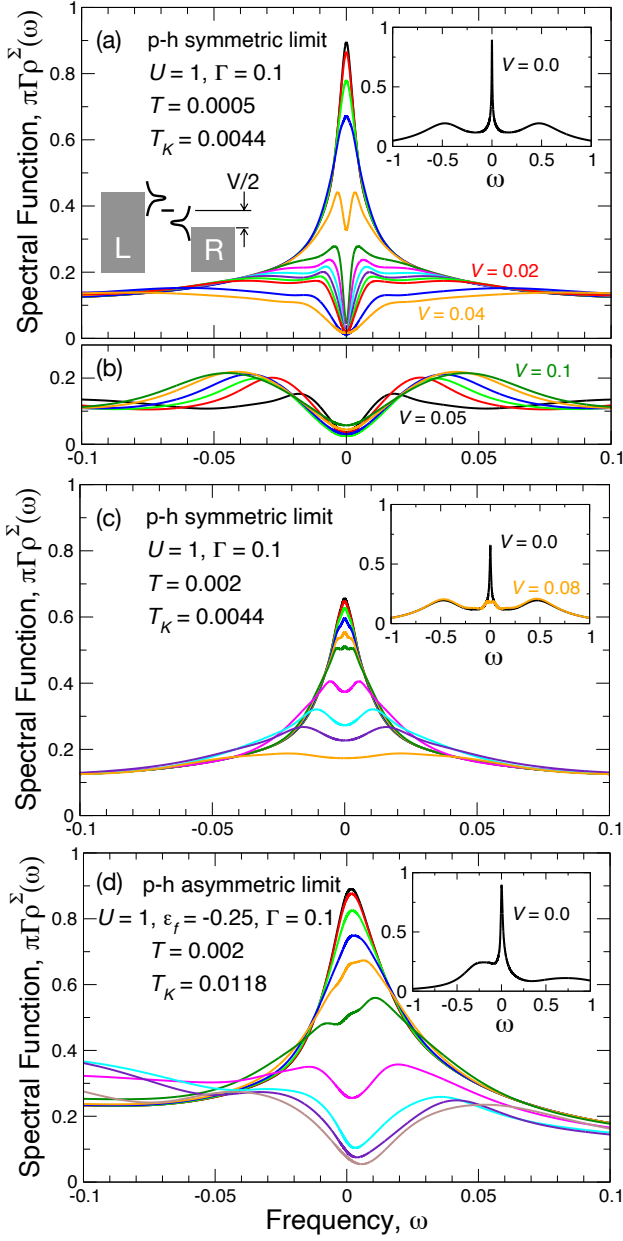


FIG. 4. Spectral evolution of Anderson model under bias. (a) Particle-hole (p-h) symmetric limit with $\epsilon_f = 0$ in the strong Kondo regime ($U/\Gamma = 10$, $\Gamma = \Gamma_L + \Gamma_R$) at a temperature much lower than the Kondo temperature T_K . The right inset shows the whole frequency range demonstrating the sharpness of the Kondo resonance. The left inset depicts the Kondo resonance attached to each lead. From top to bottom, the bias is $V = 0.0, 0.002, 0.004, 0.006, 0.008, 0.01, 0.012, 0.014, 0.016, 0.018, 0.02$ (red), 0.03 , and 0.04 (orange). (b) Peak splitting at large bias $V \lesssim \Gamma$. The position of the side-peaks is at $\pm V/2$. $V = 0.05$ (black) to 0.1 (green) with the steps of $\Delta V = 0.01$. (c) Same as (a) and (b) at temperature $T \approx 0.5T_K$. The features smeared rapidly and the sharp spectral dip disappeared, consistent with the literature. $V = 0$ (top), $0.002, 0.004, 0.006, 0.008, 0.01, 0.2, 0.4, 0.6$, and 0.8 (bottom). (d) p-h asymmetric limit ($\epsilon_f = U/4$). $V = 0$ (top), $0.005, 0.01, 0.015, 0.02, 0.03, 0.04, 0.05, 0.06$, and 0.1 (bottom).

frequency structure, the (inverse) time-evolution scale η in Eq. (4) must be small, as

$$\eta = 0.1 \times \max(T_K, T, V/2) \quad (8)$$

with $\eta \ll T_K$ for $T, V \ll T_K$. Only when $\eta \ll T_K$ the spectral functions $\rho^\Sigma(\omega)$ and $\rho(\omega)$ agree for $|\omega| \ll T_K$. This points to the fact that the time-evolution should be taken much longer than the inverse of the emergent energy scale to describe correlated nonequilibrium. (See SM [22] for further discussion.)

This strong split of the Kondo peak may be attributed to the splitting of the original Kondo resonance with the total hybridization $\Gamma_L + \Gamma_R$ to much narrower resonances resolved to each lead with the reduced hybridization $\Gamma_L (= \Gamma_R)$, as depicted in the left inset. Since the split resonance has a much narrower energy scale than T_K , internal spectral structures emerge inside the original envelope of the width T_K . The spectral dip is reminiscent of the two-channel Kondo model [31, 32], where the bias possibly breaks the symmetry between the charge- and spin-(flavor) fermions [33], pushing the single-channel towards the two-channel Kondo limit.

As V increases further, as shown in (b), the peak becomes decorrelated and the position aligns well at $\pm V/2$. Even though those peaks are often referred to as split Kondo peaks, their linewidth is much greater than T_K and they should be considered weakly correlated.

The spectral evolution is sensitive to temperature, as shown in Fig. 4(c). At an increased T from (a) yet $T < T_K$, the thermal excitations across the sub-Kondo peaks nearly smear out the structures shown in (a) and recover the spectral features previously reported in literature [7, 10, 11]. It is unlikely that the strong sub-Kondo splitting in (a) cannot be attributed to the insufficient number of NRG-kept states. The NRG is an iterative diagonalization scheme defined on the many-particle basis where all operators are linear and the eigenvalues to \hat{H} are independent of the statistical distribution. The lack of a dip in (c) shows that there are sufficient states to sample excitations near $\omega = 0$. (Corroborating argument with asymmetric hybridization is given in SM [22].) Fig. 4(d) demonstrates a p-h asymmetric limit with similar behaviors as the p-h symmetric case.

Strong spectral evolution results in unusual transport properties, as shown in Fig. 5. The distribution function, $f(\omega) = (2\pi i)^{-1} G_f^<(\omega)/\rho(\omega)$ with the f -level lesser Green's function $G_f^<(\omega)$, starts as the Fermi-Dirac function at zero bias (black) and, as soon as the sub-Kondo splitting occurs, it displays a strong athermal distribution at $V = 0.01$ (red). This population inversion persists up to the maximum voltage shown in Fig. 4(a). The mechanism for the population inversion is that the sub-Kondo peak at positive frequency is associated with the source (L) and receives electron population and the negative peak receives hole population from the drain (R). This

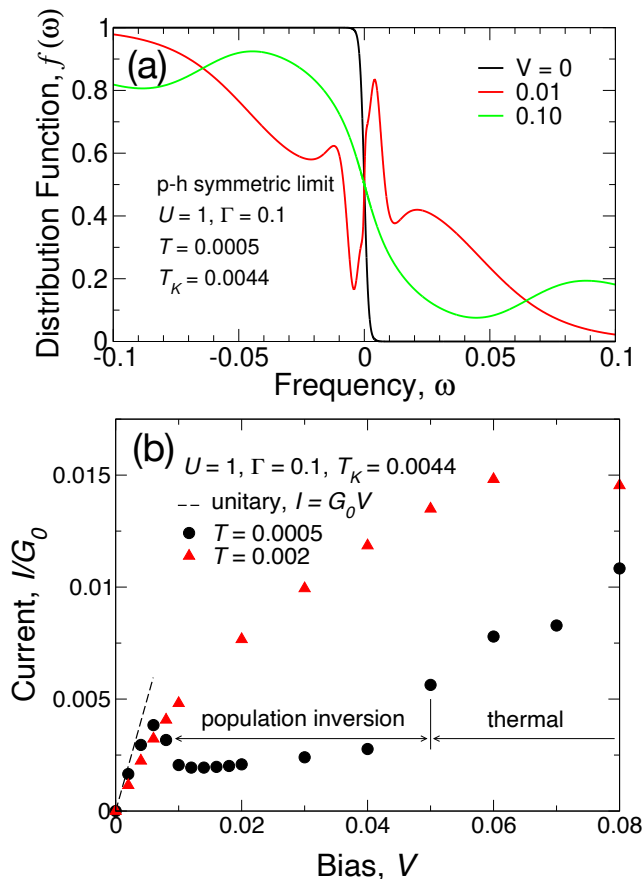


FIG. 5. The distribution function at three distinct biases. At $V = 0$ (black), the distribution is Fermi-Dirac-like. In the regime $V/2 \sim T_K$ ($V = 0.1$, red), the population in the split Kondo resonance is inverted. At larger bias $V/2 \gg T_K$ ($V = 0.1$, green), the distribution recovers to a thermal form with a positive slope at $\omega = 0$. (b) IV relation with negative differential conductance in the low- T limit at bias $V/2 \approx T_K$ ($T = 0.0005$). At higher T , thermal behavior is recovered. The dashed line is the unitary limit.

dissociation of the lead-resolved sub-Kondo resonance is also indicative of the two-channel physics.

As the voltage enters the decorrelated regime of Fig. 4(b), the distribution reverts to a thermal distribution. At a higher temperature [$T = 0.002$ not shown in (a)], there is a strong mix between the sub-Kondo peaks and the distribution is thermal at all voltage. The current, evaluated from the Dyson equations [23], directly bears out the effect of the population inversion. While the linear response theory always holds up in the zero bias limit, a negative differential conductance appears at $V/2 \approx T_K$ followed by a slow increase of current [34]. After the distribution reverts to a thermal form, the current increases rapidly. At a higher temperature $T = 0.002$, the IV shows an activated transport with a gradual deviation from the linear response behavior, as expected.

Reformulation of the scattering theory with modified full-density-matrix numerical renormalization group method reveals lead-resolved sub-Kondo structures at bias $V \sim T_K$ and temperature $T \ll T_K$ (with the Kondo temperature T_K), suggestive of an emergent two-channel nonequilibrium physics. The nonequilibrium distribution is strongly athermal and results in unusual transport behaviors.

The author thanks F. Anders, E. Arrigoni, H. Fotsos, G. Kotliar, and A. Weichselbaum for helpful discussions. Computational support from the CCR at the University at Buffalo is acknowledged.

* jonghan@buffalo.edu

- [1] J. Kondo, Resistance minimum in dilute magnetic alloys, *Prog. Theor. Phys.* **32**, 37 (1964).
- [2] A. C. Hewson, *The Kondo Problem to Heavy Fermions*, Cambridge Studies in Magnetism (Cambridge University Press, 1997).
- [3] B. Doyon and N. Andrei, Universal aspects of nonequilibrium currents in a quantum dot, *Phys. Rev. B* **73**, 245326 (2006).
- [4] P. Mehta and N. Andrei, Nonequilibrium transport in quantum impurity models: The bethe ansatz for open systems, *Phys. Rev. Lett.* **96**, 216802 (2006).
- [5] Y. Meir, N. Wingreen, and P. Lee, Low-temperature transport through a quantum dot: The anderson model out of equilibrium, *Phys. Rev. Lett.* **70**, 2601 (1993).
- [6] K. Ueda, Perturbative approach to the nonequilibrium kondo effect in a quantum dot, *Phys. Rev. B* **68**, 155310 (2003).
- [7] A. Erpenbeck, E. Gull, and G. Cohen, Quantum Monte Carlo method in the steady state, *Phys. Rev. Lett.* **130**, 186301 (2023).
- [8] J. E. Han and R. J. Heary, Imaginary-time formulation of steady-state nonequilibrium: Application to strongly correlated transport, *Phys. Rev. Lett.* **99**, 236808 (2007).
- [9] E. Arrigoni, M. Knap, and W. von der Linden, Nonequilibrium dynamical mean-field theory: An auxiliary quantum master equation approach, *Phys. Rev. Lett.* **110**, 086403 (2013).
- [10] A. Dorda, M. Nuss, W. von der Linden, and E. Arrigoni, Auxiliary master equation approach to nonequilibrium correlated impurities, *Phys. Rev. B* **89**, 165105 (2014).
- [11] F. B. Anders, Steady-state currents through nanodevices: A scattering-states numerical renormalization-group approach to open quantum systems, *Phys. Rev. Lett.* **101**, 066804 (2008).
- [12] A. Georges, G. Kotliar, W. Krauth, and M. Rozenberg, Dynamical mean-field theory of strongly correlated fermion systems and the limit of infinite dimensions, *Rev. Mod. Phys.* **68**, 13 (1996).
- [13] H. Aoki, N. Tsuji, M. Eckstein, M. Kollar, T. Oka, and P. Werner, Nonequilibrium dynamical mean-field theory and its applications, *Rev. Mod. Phys.* **86**, 779 (2014).
- [14] A. Oguri, Fermi liquid theory for the nonequilibrium Kondo effect at low bias voltages, *J. Phys. Soc. Jap.* **74**, 110 (2005).

- [15] J. E. Han, Imaginary-time formulation of steady-state nonequilibrium in quantum dot models, *Phys. Rev. B* **81**, 245107 (2010).
- [16] S. Hershfield, Reformulation of steady state nonequilibrium quantum statistical mechanics, *Phys. Rev. Lett.* **70**, 2134 (1993).
- [17] E. Merzbacher, *Quantum Mechanics* (John Wiley & Sons, New York, 1998).
- [18] M. Gell-Mann and M. Goldberger, The formal theory of scattering, *Phys. Rev.* **91**, 398 (1953).
- [19] K. G. Wilson, The renormalization group: Critical phenomena and the Kondo problem, *Rev. Mod. Phys.* **47**, 773 (1975).
- [20] H. R. Krishna-Murthy, J. W. Wilkins, and K. G. Wilson, Renormalization-group approach to the Anderson model of dilute magnetic alloys. I. Static properties for the symmetric case, *Phys. Rev. B* **21**, 1003 (1980).
- [21] R. Bulla, T. A. Costi, and T. Pruschke, Numerical renormalization group method for quantum impurity systems, *Rev. Mod. Phys.* **80**, 395 (2008).
- [22] Supplementary Material.
- [23] Y. Meir and N. Wingreen, Landauer formula for the current through an interacting electron region, *Phys. Rev. Lett.* **68**, 2512 (1992).
- [24] F. Anders and A. Schiller, Real-time dynamics in quantum-impurity systems: A time-dependent numerical renormalization-group approach, *Phys. Rev. Lett.* **95**, 196801 (2005).
- [25] A. Weichselbaum and J. Von Delft, Sum-rule conserving spectral functions from the numerical renormalization group, *Phys. Rev. Lett.* **99**, 076402 (2007).
- [26] W. Hofstetter, Generalized numerical renormalization group for dynamical quantities, *Phys. Rev. Lett.* **85**, 1508 (2000).
- [27] O. Sakai, Y. Shimizu, and T. Kasuya, Single-particle and magnetic excitation spectra of degenerate Anderson model with finite f - f Coulomb interaction, *J. Phys. Soc. Jap.* **58**, 3666 (1989), <https://doi.org/10.1143/JPSJ.58.3666>.
- [28] H. Krishna-murthy, J. W. Wilkins, and K. G. Wilson, Renormalization-group approach to the Anderson model of dilute magnetic alloys. II. Static properties for the asymmetric case, *Phys. Rev. B* **21**, 1044 (1980).
- [29] W. C. Oliveira and L. N. Oliveira, Generalized numerical renormalization-group method to calculate the thermodynamical properties of impurities in metals, *Phys. Rev. B* **49**, 11986 (1994).
- [30] R. Bulla, A. C. Hewson, and T. Pruschke, Numerical renormalization group calculations for the self-energy of the impurity Anderson model, *J. Phys. Condens. Matter* **10**, 8365 (1998).
- [31] P. Nozières and A. Blandin, Kondo effect in real metals, *J. Phys. (Paris)* **41**, 193 (1980).
- [32] A. I. Tóth and G. Zaránd, Dynamical correlations in the spin-half two-channel Kondo model, *Phys. Rev. B* **78**, 165130 (2008).
- [33] A. Schiller and S. Hershfield, Exactly solvable nonequilibrium Kondo problem, *Phys. Rev. B* **51**, 12896 (1995).
- [34] M. Jeannin, Y. Núñez-Fernández, T. Kloss, O. Parcollet, X. Waintal, A comprehensive study of out-of-equilibrium Kondo effect and Coulomb blockade, *arXiv:2502.16306* (2025), <https://doi.org/10.48550/arXiv.2502.16306>.

Supplementary Material: Nonequilibrium Spectral Evolution of Sub-Kondo Resonance

Jong E. Han

A. Details of spectral dip at a large η than that of Eq. (8) and with asymmetric hybridization

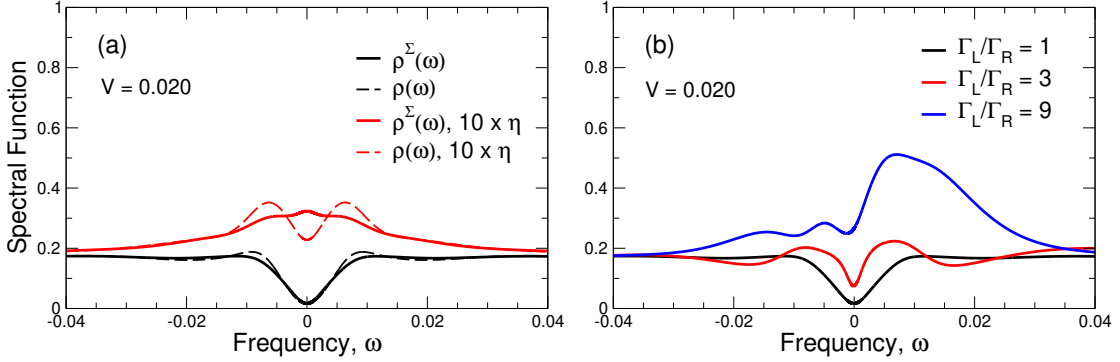


Fig. S1: Comparison of spectral functions for different η , Eq. (8), of the main text, corresponding to the parameter set for Fig. 4(a) at bias $V = 0.02$. (a) Spectral function with the self-energy trick $\rho^\Sigma(\omega)$ (solid line) and that from the direct spectral summation $\rho(\omega)$ (dashed line) with η defined as Eq. (8) (black) and with η set 10 times larger than Eq. (8) (red). (b) Comparison of $\rho^\Sigma(\omega)$ with symmetric ($\Gamma_L = \Gamma_R$) and asymmetric ($\Gamma_L > \Gamma_R$) hybridization between the L and R -leads. $\Gamma = \Gamma_L + \Gamma_R$ remains fixed. At $\Gamma_L/\Gamma_R = 9$, the dip almost disappears and the Kondo resonance is dominantly from the L -lead with the center of resonance shifted to $\sim +V/2$ and its width approaching the single-channel T_K .

The infinitesimal factor η in Eq. (4) of the main text determines the time interval during which the steady-state ensemble is established. To describe the energy scale less than the Kondo temperature T_K , η should be set much smaller than T_K , as Eq. (8). Fig. S1(a) shows that an η set 10 times larger than that in Eq. (8) results not only in an overall enhancement of the $\omega = 0$ spectral weight but also a consistent mismatch between the spectral functions of $\rho^\Sigma(\omega)$ evaluated from the self-energy trick and $\rho(\omega)$ directly computed from the spectral weight summation. The inconsistency between the two methods, especially the overestimation of $\rho^\Sigma(0)$, is persistent in the large- η limit.

Fig. S1(b) demonstrates the disappearance of the dip at $\omega = 0$ as the L - R symmetry is removed. As the ratio Γ_L/Γ_R becomes larger, the system approaches the single-reservoir physics. The size of the calculation, such as the number of kept states, remains the same throughout, and therefore, the dip in the symmetric ($\Gamma_L = \Gamma_R$) limit is not likely from the size of the NRG calculation.

B. Computational Cost

Apart from using the density-matrix Eq. (2) of the main text, in place of that from the equilibrium full-density-matrix numerical renormalization group (FDM-NRG), the structure of the algorithm is the same as the previous works [1]. The behavior of the density matrix weight and the range of energy eigenvalues as a function of the NRG chain is illustrated in Fig. S2.

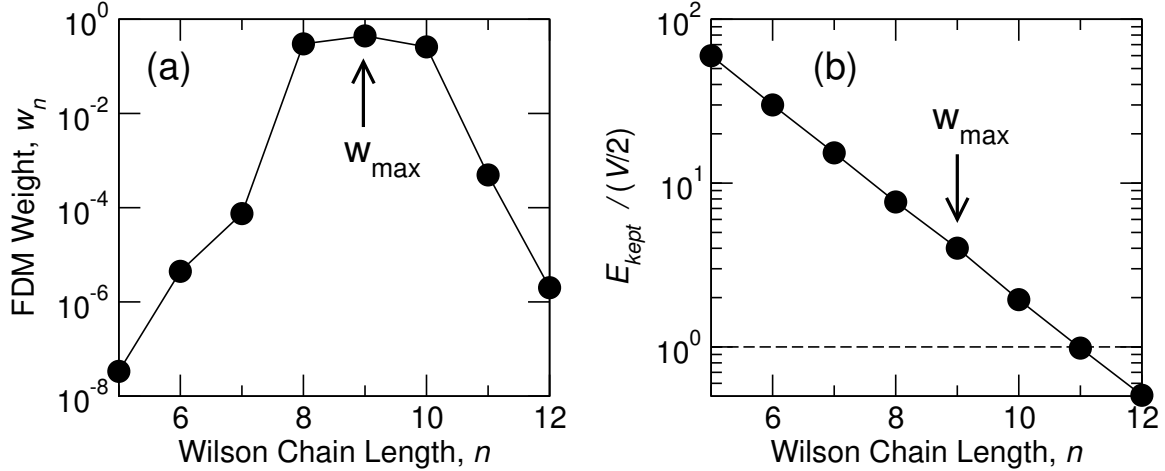


Fig. S2: (a) Full-density-matrix weight w_n as a function of the Wilson chain length n . The weight is strongly peaked around $n = 9$. Parameters are from Fig. 4(c) from the main text. (b) The maximum kept energy E_{kept} versus the bias $V/2$ with the chain length n . E_{kept} is defined in the energy scale of the unrenormalized Hamiltonian. It is desirable to have $E_{\text{kept}}/(V/2) > 1$ to cover the excited energies, which is satisfied for dominant density-matrix configurations.

In practice, the NRG iterations are repeated three times: (i) to identify the maximum weight w_n of the density matrix for the Wilson chain length n , (ii) to produce the basis transformation matrix [1, 2] to compute the reduced density-matrix, (iii) for a production run to compute observables, such as the spectral weight. With the size of the Hilbert space N_{sp} at each NRG iteration being $N_{\text{sp}} = 16N_{\text{kept}}$ (16 for the two added sites to the L - and R -Wilson chains, N_{kept} for the number of kept states from the previous iteration), the computational times for the diagonalization of the Hamiltonian \hat{H} , the construction of the Y -operator and the exponentiation of $\hat{H} - V\hat{Y}$, and the computation of the spectral coefficients scale as N_{sp}^3 . Despite the similar scaling between tasks, the third-stage NRG runs to compute matrix elements of observables are the most time-consuming, and with $N_{\text{kept}} = 1000$ and the Wilson chains up to length 10, its computation time is roughly 40 minutes on an Apple M2 processor per z value. All three stages take roughly one hour and 5 GB of memory per z value.

C. Fortran Code for Y -operator in the Non-interacting Resonant-Level Model

The Fortran code to generate Fig. 2 is shown in verbatim.

```

module types
  implicit none
  integer, parameter :: i4b=selected_int_kind(9)
  integer, parameter :: dp=kind(1.0d0)
end module types

module globals
  use types
  implicit none
  integer(i4b), parameter :: msite=80,max=2*msite+1
  real(dp) :: lambda,V,temp,D0,t0

```



```

real(dp) :: tn(-1:max),eta,current,g0,ith,h(max,max),eig(max),evec(max,max), &
          en1(max),work(20*max)
complex*16 :: yop(max,max),y0op(max,max),hy(max,max),zvec(max,max),zwork(20*max), &
             rhoneq(max,max),cij(max,max)
real(dp), parameter :: pi=2.d0*dasin(1.d0)
complex*16, parameter :: ii=(0.d0,1.d0)
end module globals
!
! =====
! Non-interacting resonant level calculation
! =====
!
program NIRLM

use types
use globals
implicit none
integer(i4b) :: i,j,k,iv,info,l
real(dp) :: sum,yR,yL
complex*16 zsum

open(5,file='input.par')
open(16,file='curr.dat')
!
! -----
! Wilson chain parameters
! -----
!
read(5,*)
read(5,*) D0,lambda,t0,temp,eta
!
do l=0,msite-1

tn(l) = 0.5d0*(1.0d0+1.0/lambda)/sqrt(lambda**(l-1))* &
        (1.0d0-lambda**(-l-1))* &
        ((1.0d0-lambda**(-2*l-1))*(1.0d0-lambda**(-2*l-3)))*(-0.5d0)
write(6,*) l,tn(l)

enddo

h = 0.0
do l=0,msite-2
i = l + msite + 2
h(i,i+1) = -tn(l)
h(i+1,i) = -tn(l)
i = -l + msite
h(i,i-1) = -tn(l)
h(i-1,i) = -tn(l)

```

```

    enddo
    h(msite+1,msite+2) = -t0
    h(msite+2,msite+1) = -t0
    h(msite+1,msite) = -t0
    h(msite,msite+1) = -t0
!
! -----
! BLAS-LAPACK routine
! -----
!
    evec = h
    call dsyev('V','U',max,evec,max,en1,work,20*max,info)

    do i=1,max
        do j=1,max
            yR = 0.0
            do k=msite+2,2*msite+1
                yR = yR + evec(k,i)*evec(k,j)
            enddo
            yL = 0.0
            do k=1,msite
                yL = yL + evec(k,i)*evec(k,j)
            enddo
            y0op(i,j) = yL-yR
        enddo
    enddo

    do i=1,max
        do j=1,max
            yop(i,j) = ii*eta/(-en1(i)+en1(j)+ii*eta)*y0op(i,j)
        enddo
    enddo

    do i=1,max
    do j=1,max
        zsum = evec(msite+1,i)*evec(msite+2,j)
        zsum = zsum - evec(msite+2,i)*evec(msite+1,j)
        zsum = zsum - evec(msite+1,i)*evec(msite,j)
        zsum = zsum + evec(msite,i)*evec(msite+1,j)
        cij(i,j) = -0.5*ii*t0*zsum
    enddo
    enddo

    do iv=0,400

        V = 0.0001*iv

```

```

hy = 0.0
do i=1,max
  hy(i,i) = en1(i)
enddo
hy = hy - 0.5*V*yop

zvec = hy

call zheev('V','U',max,zvec,max,eig,zwork,20*max,work,info)

do i=1,max
do j=1,max
  zsum = 0.0
  do k=1,max
    zsum = zsum + zvec(i,k)*dconjg(zvec(j,k))/(1.0+exp(eig(k)/temp))
  enddo
  rhoneq(i,j) = zsum
enddo
enddo

!
! -----
! zvec() contains the overlap of eigenstates of the density matrix
! to those of the Hamiltonian.
! -----
!

g0 = pi*t0**2/(2.0*D0)
ith = 4.0*g0*datan(V/(4.0*g0))/(2.0*pi)
current = 0.0
do i=1,max
  do j=1,max
    current = current + rhoneq(i,j)*cij(j,i)
  enddo
enddo
write(16,'(3f20.12)') V,2.0*pi*current,2.0*pi*ith

enddo

end program NIRLM

```

-
- [1] A. Weichselbaum and J. Von Delft, Phys. Rev. Lett. **99**, 076402 (2007).
[2] W. Hofstetter, Phys. Rev. Lett. **85**, 1508 (2000).